Global mapping and characterization of Titan's dune fields with Cassini: Correlation between RADAR and VIMS observations

Sébastien Rodriguez, A Garcia, A Lucas, T Appéré, Alice Le Gall, E Reffet, L. Le Corre, Stéphane Le Mouélic, T. Cornet, S. Courrech Du Pont, et al.

Global mapping and characterization of Titan's dune fields with Cassini: correlation between RADAR and VIMS observations

S. Rodriguez[1], A. Garcia[1], A. Lucas[1], T. Appéré[1], A. Le Gall[2], E. Reffet[1], L. Le Corre[3], S. Le Mouélic[4], T. Cornet[4], S. Courrech du Pont[5], C. Narteau[6], O. Bourgeois[4], J. Radebaugh[7], K. Arnold[7], J.W. Barnes[8], K. Stephan[9], R. Jaumann[9], C. Sotin[10], R.H. Brown[11], R.D. Lorenz[12], E.P. Turtle[12]

[1] Laboratoire Astrophysique, Instrumentation et Modélisation (AIM), CNRS-UMR 7158, Université Paris-Diderot – CEA-SACLAY, 91191 Gif sur Yvette, France (sebastien.rodriguez@cea.fr);
[2] Laboratoire Atmosphères, Milieux, Observations Spatiales (LATMOS- UVSQ), Paris, France;
[3] Planetary Science Institute, 1700 East Fort Lowell, Suite 106, Tucson, AZ 85719-2395;
[4] Laboratoire de Planétologie et Géodynamique (LPGNantes), CNRS-UMR 6112, Université de Nantes, 2 rue de la Houssinière, 44322 Nantes, France;
[5] Laboratoire Matière et Systèmes Complexes (MSC), CNRS-UMR 7057, Université Paris Diderot, Paris, France;
[6] Institut de Physique du Globe de Paris (IPGP), Laboratoire de Dynamique des Fluides Géologiques, Paris, France;
[7] Department of Geological Sciences, Brigham Young University, Provo, UT, USA;
[8] Department of Physics, University of Idaho, Moscow, ID 83844, USA;
[9] DLR, Institute of Planetary Research, Berlin, Germany;
[10] Jet propulsion Laboratory, California Institute of Technology, 4800 Oak Grove drive, Pasadena, CA 01109, USA;
[11] Department of Planetary Sciences, University of Arizona, Lunar and Planetary Laboratory, Tucson, AZ85721-0092, USA;
[12] Johns Hopkins University Applied Physics Laboratory, Laurel, MD, USA.

Corresponding author:

Sébastien Rodriguez
Laboratoire AIM – Université Paris Diderot – Paris 7, CEA-Saclay, DSM/IRFU/SAp
Centre de l'Orme des Merisiers, bât. 709
91191 Gif/Yvette Cedex France
tel. +33 (0)1 69 08 80 56
fax +33 (0)1 69 08 65 77
Email: sebastien.rodriguez@cea.fr

Running title: Mapping of Titan's dune fields with Cassini RADAR and VIMS.

Keywords: Titan, surface; Radar observations; Infrared observations; Geological processes.

Abstract

Vast fields of linear dunes have been observed in the equatorial regions of Titan, Saturn's largest moon. As the Cassini mission, in orbit around Saturn since July 2004 and extended until May 2017, carries on, the high-resolution coverage of Titan's surface increases, revealing new dune fields and allowing refinements in the examination of their properties. In this paper, we present the joint analysis of Cassini's microwave and infrared global scale observations of Titan. Integrating within an up-to-date global map of Titan all the Cassini RADAR and VIMS (Visual and Infrared Mapping Spectrometer) images – the latter being empirically corrected for atmospheric scattering and surface photometry, from July 2004 through July 2013 and June 2010 respectively, we found a very good qualitative and quantitative spatial matching between the geographic distribution of the dune fields and a specific infrared spectral unit (namely the "dark brown" unit). The high degree of spatial correlation between dunes and the "dark brown" unit has important implications for Titan's geology and climate. We found that RADAR-mapped dunes and the "dark brown" unit are similarly confined within the equatorial belt (±30° in latitudes) with an equivalent distribution with latitude, suggesting an increasing sediment availability and mobility at Titan's tropics relative to higher latitudes, compatible with the lower ground humidity predicted in equatorial regions by General Circulation Models. Furthermore, the strong correlation between RADAR-mapped dunes and the VIMS "dark brown" unit (72%) allows us to better constrain the total surface area covered by dune material, previously estimated from the extrapolation of the RADAR observations alone. According to our calculations, dune material cover 17.5 ± 1.5% of Titan's surface area, equivalent to a total surface area of 14.6 ± 1.2 million km^2 (~1.5 times the surface area of Earth's Sahara desert). The VIMS "dark brown" coloration of the dune material is here confirmed at large spatial scale. If the sand particle composition is

63 dominated by solid organics produced in and settling from the atmosphere, as supported by
64 our spectral modeling and by previous spectral analysis, microwave radiometric data and
65 atmospheric modeling, dune fields are one of the major surface hydrocarbon reservoirs on
66 Titan. Assuming two possible scenarios for the sand distribution (either the sand is (1) entirely
67 trapped in dune landforms, or (2) trapped in dunes at places where dune landforms are firmly
68 observed and in sand sheets elsewhere), we estimate the volume of hydrocarbons trapped in
69 the dune sediment to be comprised between 1.7 and 4.4×10^5 km^3, corresponding to an average
70 total mass of 230,000 GT, in comparison with ~4,000-30,000 GT of hydrocarbons in the polar
71 lakes and seas. This indicates a maximum age for the dune sediments of ~730-Myr, consistent
72 with estimations of the ages of the current Titan's atmospheric methane and surface.
73

1. Introduction.

Saturn's largest moon Titan has a cold, hazy, dense nitrogen- and hydrocarbon-rich atmosphere. This planet-sized icy moon has a complex climatic system (see Lebonnois et al., 2009 for a review), with hydrocarbon seasonal cycles including clouds (Rodriguez et al., 2009, 2011; Brown et al., 2010; Turtle et al., 2009, 2011a; Le Mouélic et al., 2011) and rainfall (Turtle et al., 2011b; Barnes et al., 2013), that globally tends to transport humidity from the equator to the poles (Rannou et al., 2006; Mitchell et al., 2006; Mitchell, 2008; Schneider et al., 2012). Since 2004, the Cassini orbiter has been continuously providing a wealth of images of the surface of Titan at different wavelengths and with unprecedented resolution (down to ~200 m for the RADAR imager). Images from the ISS (Imaging Science Sub-system) cameras, the VIMS (Visual and Infrared Mapping Spectrometer) instrument and the RADAR experiment in SAR (Synthetic Aperture Radar) mode, all on board the Cassini spacecraft, have revealed the presence of landforms strongly linked to the climatic activity of the moon: hydrocarbon lakes and seas at high latitudes (e.g. Stofan et al., 2007), complex networks of fluvial channels at all latitudes (e.g. Elachi et al., 2006) and vast fields of dunes mostly around the Equator (e.g. Lorenz et al., 2006). The latitudinal distribution of these features is indicative of the different types of climates that Titan experiences or has experienced in the past. Dunes, in particular, provide a powerful tool to investigate the sedimentary and climatic history of the arid and/or semi-arid environments likely to prevail at Titan's tropics.

The thousands of dunes observed by Cassini on the surface of Titan, globally organized in vast dune fields, are mainly confined to the equatorial belt, within ±30° in latitude, and almost encircle the globe in longitude, except in the Xanadu region (70°W-140°W, e.g. Radebaugh et al., 2011) where dunes are absent. The high resolution RADAR

SAR images allowed estimation of their main morphological properties. Titan's dunes have a width of ~1 km, a spacing of 1-3 km, lengths of many tens to a few hundreds of km (Lorenz et al., 2006; Radebaugh et al., 2008; Lorenz and Radebaugh, 2009), and their heights have been estimated by photo- and radar-clinometry to ~100 m (Barnes et al., 2008; Neish et al., 2010). Nearly all of them are radar-dark, linear in form and similar in size and morphology to linear dunes typically found in large sand seas on Earth, *e.g.* in the Namib, Chinese or Saudi Arabian deserts (Lancaster, 1995). Cassini VIMS and RADAR observations at lower resolution have also shown that both the infrared behavior and the microwave emission from the dune fields are strongly suspected to be compatible with "sand" particles most likely dominated by solid organics, spectrally similar to atmospheric aerosols (Soderblom et al., 2007; Barnes et al., 2008; Clark et al., 2010; Le Gall et al., 2011; Hirtzig et al., 2013). The mechanical properties of Titan's dunes and their formation mechanism have also been investigated. Titan's low gravity (1.35 m/s^2) and slightly denser atmosphere than Earth's (1.47×10^5 Pa) increase the mobility of particles. The theoretical "fluid" threshold friction speed required to initiate the formation of dunes (through the saltation of particles) under Titan's condition has been calculated as 0.03 to 0.06 m/s (which corresponds to "real" near-surface wind speeds of 0.8-1.5 m/s), with an optimum saltation diameter of 200-600 µm depending on the bulk composition of particles (Greeley and Iversen, 1985; Allison, 1992; Lorenz et al., 1995, 2006; Kok et al., 2012; with an extended review in Lorenz, 2013). Kok et al. (2012) also defined the "impact" threshold as the threshold friction speed needed to sustain saltation. They calculated the "impact" threshold for Titan and showed that the ratio of the "impact" to "fluid" threshold speeds is greater than unity (as for Venus, but contrary to Earth and Mars). Saltation on Titan therefore needs greater winds to be sustained than to be initiated, primarily due to the thicker atmosphere which efficiently dissipates the vertical motion of saltating particles (Kok et al., 2012). The presence of dunes at Titan's tropics thus

123 indicates (1) the production of a sufficient supply of saltatable particles, probably originated
124 as photochemical end-products settling directly from the atmosphere, (2) the generation of
125 winds capable of moving sand-sized particles by saltation, and (3) conditions dry enough to
126 allow sand transport near equatorial latitudes.

127 The complex interplay between the hydrocarbon cycle and surface processes leading
128 to the formation and dynamics of Titan's dunes, however, is far from being fully understood.
129 The precise composition and mechanical properties of the dune sediment, its origins, sources,
130 geographic coverage and total volume are still open questions that require further
131 investigation. The total volume of organic sediment trapped in the dunes has been roughly
132 evaluated to be between ~10^4 and 10^5 km^3 by Lorenz et al. (2006), by extrapolation of the
133 area that dunes cover in the two RADAR SAR swaths acquired in February and October 2005
134 and thanks to their apparent correlation with the large infrared-dark regions found by ISS in
135 equatorial regions. Subsequent SAR observations indicated that dunes may cover as much as
136 20% of Titan's total surface area (up to 40% of equatorial areas) (Radebaugh et al., 2008),
137 allowing a re-evaluation of the total volume of sand-sized sediment between 2 and $8x10^5$ km^3
138 (Lorenz et al., 2008), suggesting that the dune system represents a major surface geologic
139 feature. These numbers were recently updated by Le Gall et al. (2011) compiling the 27
140 RADAR SAR images available at that time, resulting, in a new estimate of the total surface
141 area covered by dunes (~11-12.5%) and sediment volume ($0.5\text{-}5x10^5$ km^3) by extrapolating
142 the partial RADAR coverage to the whole surface of Titan.

143 Combining data from RADAR and infrared experiments from the Cassini orbiter
144 offers an extraordinary powerful and complementary tool to explore the surface of Titan. It
145 allows to jointly benefit from the high resolution of the SAR images on one side (enough to
146 resolve individual dunes) and from the spectral and spatial coverage of the ISS and VIMS

observations on the other side. The combined use of microwave and infrared observations of Titan therefore allows not only to better constrain and quantify the total dune coverage, but also to provide more quantitative clues to their composition. Soderblom et al. (2007) and Barnes et al. (2008) were the first to thoroughly investigate the degree of correlation between infrared spectral units identified with VIMS and RADAR images of Titan's dunes. At regional scale, they clearly demonstrated that SAR dunes strongly correlate with a specific spectral unit showing up mainly in the equatorial belt in VIMS mosaics (the "dark brown" unit, suspected to be water ice poor – Barnes et al., 2007, 2008; Soderblom et al., 2007; Le Mouélic et al., 2008). Extending the work of Soderblom et al. (2007) and Barnes et al. (2008) at Titan's globe scale, Le Corre et al. (2008) calculated the correlation between SAR dunes and the VIMS "dark brown" unit to be more than 80%, inferring a total dune coverage of ~18% and a total "sand" volume of ~$3x10^5$ km^3. Although in agreement with both previous and following calculations, estimates of Le Corre et al. (2008) were obtained from a very preliminary study with only a limited set of observations (up to 2007 for RADAR SAR – from TA to T25 – and 2008 for VIMS observations – from TA to T42). Recently, Arnold et al. (2013) explored in a single sand sea the possible correlation between dunes seen in RADAR images and albedo units at 0.938 µm in ISS images, extending the previous work of Lorenz et al. (2006). They found good qualitative correlation between dunes and the darkest ISS areas within a test zone located in Fensal and Aztlan areas. Using the global RADAR/ISS image coverage and the total sand area from RADAR and ISS in Fensal and Aztlan areas (2.3 million km^2), they extrapolated the total sand coverage on Titan to 14%, or 12 million km^2, close to the calculation of Le Gall et al. (2011). Arnold et al. (2013) also gave a new estimate of 1.5-$3x10^5$ km^3 for the global sand volume.

As illustrated by the fluctuations in all the sediment volume estimates, despite the extensive body of work in mapping Titan's dunes, calculating the areas of the sand seas is very challenging given the partial coverage of RADAR images and low resolution of ISS/VIMS observations. Besides, the accurate analysis of infrared observations of Titan's surface is made complex due to the strong atmospheric contributions (gaseous absorption and haze scattering), especially at short infrared wavelengths (below 3 µm). Thus, as Cassini will continue to observe Titan up to May 2017, one must take advantage of any significant progress in the coverage and method of processing of SAR and infrared data. Following the pioneering work of Soderblom et al. (2007), Barnes et al. (2008) and Le Corre et al. (2008), we present here detailed mapping and characterization of Titan's dune fields at the global scale, using an importantly extended set of RADAR and VIMS images (section 2). Doing so, we significantly update the geographic distribution and the estimate of the total coverage of the dunes, and refine the correlation of different types of data (RADAR/SAR and VIMS) and the inventory of solid organics on Titan (section 3). On this purpose, we use here a full global mosaic of VIMS images of Titan's surface empirically corrected for atmospheric contributions. The correlation between the dunes imaged by the RADAR/SAR and some infrared spectral units appearing in VIMS observations also provides new constraints on the dune compositional properties (section 3).

2. Global mapping of the dunes.

2.1 Dune global mapping with the RADAR SAR data.

The Cassini RADAR instrument is a microwave sensor operating at a frequency of 13.78 GHz (λ=2.17 cm, Ku band) and having three active (altimeter, scatterometer and

193 synthetic aperture radar, or SAR) and one passive working modes (radiometer) (Elachi et al.,
194 2004).

195 For our mapping purposes, we restricted this study to datasets acquired by the SAR
196 imaging mode of the Cassini RADAR. Depending on the altitude of Cassini during
197 acquisition, RADAR images provide the best spatial sampling of the Cassini remote sensing
198 payload when observing Titan, ranging from 0.2 to 2 km/pixel for the "regular" SAR mode,
199 when the spacecraft is at closest approach, i.e. between 1,000 and 4,000 km altitude. RADAR
200 images can also be acquired for altitudes greater than 10,000 km. The RADAR is thus
201 operating in the "High-altitude" SAR mode (also called HiSAR) and the resulting spatial
202 sampling is lower, typically >1 km/pixel (possibly up to ~20km/pixel). The RADAR imaging
203 mode results in the production of swaths 120 to 450 km-wide, at Cassini altitude of 1,000 to
204 4,000 km, and about 5,000 km-long following the track of the spacecraft (Elachi et al., 2004).

205 **Figure 1a** presents the map of Titan's surface obtained by mosaicking all the SAR and
206 HiSAR images recorded between Titan's first close flyby TA (October 26th 2004) and flyby
207 T92 (July 10th 2013), putting together a total of 149 individual images (46 SAR and 103
208 HiSAR images). This corresponds to an addition of 19 individual SAR images (and of all the
209 HiSAR images) as compared to the dataset used by Le Gall et al. (2011) to map Titan's dunes.
210 All the RADAR swaths have been reprojected into the sinusoidal equal area coordinate
211 system (guaranteeing a simple and rigorous area calculation) and simple cylindrical
212 coordinate system (only for visualization purposes) using the ISIS software (Integrated
213 Software for Imagers and Spectrometers, Anderson et al., 2004) and then incorporated in a
214 Geographic Information System (GIS). Relative co-registration errors between swaths are
215 small, never exceeding ~0.1-0.2° in latitude or longitude.

Thanks to their integration into the GIS, the surface area of each individual swath has been automatically calculated (see 3rd column of **Table 1**), updating and extending the previous evaluations of Le Gall et al. (2011) and allowing the precise determination of the total surface area observed by the RADAR. At the end of July 2013, 43.1% (~35,900,000 km^2) of Titan's surface was thus covered by the highest spatial resolution SAR images. This increases by ~10% the total surface coverage of SAR observations estimated from the map drawn by Le Gall et al., 2011. The RADAR coverage is further extended up to 58.4% (~48,700,000 km^2) if all the SAR and HiSAR images are incorporated (**Figure 1a**).

[Figure 1 – full page, landscape]

The spatial resolution of the SAR images allows individual dunes to be resolved, permitting the accurate identification and delineation of the dune regions, taking into account the exclusion of the radar-bright "inselbergs" or patches embedded within the dune fields (**Figure 1b and inset**). It has been also possible to outline some more dunes within the lower-resolution HiSAR observations, but only for those down to 1.5-2 km/pixel of spatial sampling (which is the critical minimum limit of spatial sampling in order to resolve kilometer-sized features). As we manually outline dune fields, this results in small but unavoidable errors in the calculation of their total surface area. The visual uncertainty has been evaluated by drawing several times the geographic limits of dune fields over the same region. This leads to a conservative systematic uncertainty on the dune coverage and absolute surface area of 2%.

In the 2004-2013 period, dunes appear in 27 SAR and 7 HiSAR images (**Table 1**), mainly at the tropics with no apparent longitudinal preference (except for the total absence of

dunes in the Xanadu area). A few isolated dune-like features are detected at latitudes higher than 30°, in the southern (~40°S, ~35°E) and northern hemisphere (~50°N, ~45°W), the latter having been already reported by Radebaugh et al. (2012). We evaluate that dunes cover 13 ± 2% of the 58.1% of Titan's surface covered by the SAR and HiSAR observations, considering only images having a sufficient spatial resolution to identify individual dunes by excluding HiSAR swaths with resolution coarser than 2 km/pixel (accounting for 0.3% of Titan's surface coverage), and taking into account the overlap between images and dunes observed on these images. 99.6% of the imaged dunes are found within the equatorial belt (within ±30° latitudes). The dune coverage as strictly observed by the RADAR thus represents a total surface area of 6,500,000 ± 130,000 km^2. This increases by almost a factor 2 the total area of dunes firmly observed at Titan's surface (compared to the previous estimate of Le Gall et al. (2011)), especially thanks to the addition of the T77 "equatorial" SAR swath which contains 72% of dunes (**Table 1**). A direct extrapolation from the RADAR fragmentary observations alone suggests that dunes may cover more than ~23% of Titan's total surface area, equivalent to ~19.2 million km^2 (more than 2 times greater than the Sahara desert surface area), or at least ~22 % (~18.3 million km^2) if the dunes are confined within the equatorial belt (±30° latitudes), 61.3% of which has been imaged after T92. **Table 1** summarizes the information on the coverage, and the average latitude and longitude of all the dune fields that we have identified in the SAR and HiSAR swaths between TA (October 2004) and T92 flybys (July 2013).

2.2 Infrared global mapping with the VIMS instrument and extraction of spectral units.

In order to complement the mapping of Titan's surface, we also built a global mosaic of surface observations recorded in the infrared by the VIMS instrument on board Cassini.

263 The VIMS instrument is a camera that acquires images in 352 separate wavelengths and
264 produces hyperspectral cubes (Brown et al., 2004). It is composed of two distinct detectors,
265 VIMS-VIS in the visible (96 channels from 0.35 to 1.04 µm) with a spectral sampling of 7.3
266 nm, and VIMS-IR in the near-infrared (256 channels from 0.88 to 5.11 µm) with a spectral
267 sampling of 16.6 nm. VIMS-IR is able to see Titan's surface in seven narrow atmospheric
268 windows of weakest gaseous absorption (the "methane" windows) centered at 0.93, 1.08,
269 1.27, 1.59, 2.03, 2.7–2.8 and 5 µm (Sotin et al., 2005). VIMS data that we use in this study are
270 reduced to I/F using the VIMS calibration pipeline, as described in Barnes et al. (2007).

271

272 **[Figure 2 – full page, landscape]**

273

274 **[Figure 3 – single column]**

275

276 All methane windows at wavelengths shorter than 5 µm are strongly affected by
277 atmospheric scattering due to the aerosols present in Titan's atmosphere – which blurs and
278 masks the details of the surface – whereas the 5 µm window can be considered at first order as
279 free of any haze scattering (Rodriguez et al., 2006). Atmospheric contribution, along with
280 surface photometric behavior, result in significant artifacts expressed as seams in raw global
281 mosaics because they are both highly dependent on the variation of the viewing conditions
282 (incidence, emission, and phase angles).

283 **Figure 2a** shows a color composite global mosaic of Titan's surface incorporating all
284 VIMS observations between TA (October 26th, 2004) and T70 (June 21st, 2010), adding

observations acquired during 28 extra Titan's flybys since the study of Le Corre et al. (2008). This noticeably extends the coverage and improves the average resolution of the equatorial regions. Furthermore, unlike the VIMS global mosaic of Le Corre et al. (2008), the map used in this study has been produced applying the heuristic correction method for atmospheric contribution and surface photometry described in Le Mouélic et al. (2012) and Cornet et al. (2012). This method, which includes recent refinements of the surface photometric function from Cornet et al. (2013), is based on empirical corrections (applied at the center of each methane window) for (1) the atmospheric scattering effects present in the short-wavelength methane windows, and (2) the surface photometry. Those corrections allow to globally homogenize the infrared map by diminishing the occurrence of seams, and significantly enhance subtle spectral heterogeneities between surface terrains, which are otherwise damped by atmospheric scattering, by getting closer to the true surface albedo.

As shown in **Figure 2a**, at the end of June 2010, VIMS observations entirely covered the equatorial belt of Titan, with an average spatial resolution of ~15 km (see also Le Mouélic et al., 2012). Titan's polar coverage with VIMS is also complete at a low spatial resolution, but does not appear in **Figure 2a** as observations with the most extreme illumination and/or observation geometries were automatically filtered out by the correction algorithm (Le Mouélic et al., 2012). The VIMS map shows that equatorial regions are mostly dominated by three main spectral units, whose contrast is particularly enhanced thanks to our empirical corrections. Using a specific color scheme with red as the 5-µm corrected channel, green as the 2.01-µm corrected channel and blue as the 1.27-µm corrected channel, the three spectral units visually appear, respectively (1) "bright" (the Xanadu area being part of it), (2) "dark brown", and (3) "dark blue" (**Figure 2a**), the last two having been long suspected to be strongly linked to equatorial dune fields (Soderblom et al., 2007; Barnes et al., 2008).

We searched for spectral criteria to automatically extract the infrared "dark brown" and "dark blue" units from the corrected VIMS global map. Obvious advantages of this method are to avoid visual biases and to guarantee the spectral and physical consistency of the extracted areas. As we focus on the equatorial belt, all the regions poleward of ±40° in latitudes have been excluded from the extraction process. Besides, the equatorial regions benefit from the most favorable illumination and observation geometries, and therefore are where the atmospheric correction algorithm produces its best results. Looking at the spectra, "dark brown" and "dark blue" units are both characterized by very low I/F in all the atmospheric windows compared to the equatorial "bright" unit and can be easily discriminated from the brightest terrains by simply applying I/F thresholds. "Dark brown" and "dark blue" units are further separated owing to their subtle but discernible spectral differences, especially at the shortest wavelengths (below 3 µm). Indeed, "dark brown" spectra have a greater spectral slope between 1.59 and 2.78 µm than between 1.27 and 2.01 µm, which is the exact opposite spectral behavior of the "dark blue" spectra. "Dark brown" spectra also systematically exhibit lower 1.27/1.59 µm and 1.27/2.01 µm ratios than the "dark blue's". Given all those criteria, we were able to automatically isolate the two dark "units" (**Figure 2b**), which match extremely well the visual boundaries of the brownish and bluish areas of the VIMS mosaic (**Figure 2a**), and calculate their respective surface areas. As the visual transition between spectral colors is slightly fuzzy, whose sharpness is mainly limited by the average resolution of the global mosaic, i.e. ~15 km, the localization of the spectral unit edges, and the subsequent calculation of their surface areas, suffer from uncertainties. This source of error has been evaluated by conservatively expanding and shrinking the borders of the spectral units by one 'unit' of average resolution (15 km). We thus estimate that the "dark brown" and "dark blue" units cover 17.5 ± 1.5 % (14,600,000 ± 1,200,000 km^2) and 1 ± 0.5 % (840,000 ± 410,000 km^2) of the total Titan's surface area respectively.

334 **Figure 3a** shows the two infrared spectra extracted and averaged over the entire "dark
335 brown" and "dark blue" units. These spectra are each built by combining the values of I/F in
336 the five atmospheric windows from 1.27 up to 5 µm, all corrected for atmospheric
337 contribution. Even after the averaging over a very large number of spectra (more than 460,000
338 for the "dark brown" unit and more than 25,000 for the "dark blue" unit), the two resulting
339 spectra still present substantial differences. The spectrum of the "dark blue" unit is
340 significantly brighter at 1.27 µm, slightly brighter at 1.59 µm, and slightly darker at 2.01, 2.75
341 and 5 µm than the spectrum of the "dark brown" unit. When we represent the spectral slopes
342 1.27/1.59 vs 1.27/2.01 µm scatterplot for the two units (**Figure 3b**), the spectral differences
343 appear even clearer. In the scatterplot, the two units are both well confined in two small
344 clusters with only few overlaps. This is indicative of two important properties for those
345 spectral units: (1) the fact that the two units are confined in two distinct clusters in the
346 scatterplot strongly suggests that they are representative of two different classes of surface
347 composition, and (2) the fact that their spectra lie each in narrowed clusters shows that the
348 two units have intrinsically a very high degree of spectral homogeneity, indicating that the
349 two units are each covered by the same type of material.

350 As the spectra of the "dark brown" and "dark blue" units are all corrected for the
351 atmospheric contribution (following the approach of Le Mouélic et al. (2012)), this allowed us
352 to investigate further their most probable compositions. We calculated synthetic I/F spectra of
353 intimate and linear (or geographic) mixtures of granular surface composed of water ice and
354 tholins (laboratory analogues to the atmospheric solid organics constituting Titan's settling
355 haze). These synthetic spectra are computed for the average geometries of the "dark brown"
356 and "dark blue" units, by using the formalism developed by Hapke (1993) and Lucey (1998),
357 including a Henyey-Greenstein phase function for the grains and multiple scattering between

358 grains. The asymmetry factor for the grain phase function has been set to -0.4 (Buratti et al.,
359 2006) and the average grain radius has been fixed at 50 µm. We used the refractive indexes
360 measured by Warren (1984) for water ice and Khare et al. (1984) for tholins. Spectral slopes
361 of the "dark brown" and "dark blue" units are thus compared with spectral slopes predicted
362 from the granular surface modeling (**Figure 3b**). The matching between observed and
363 simulated slopes is sufficiently close to be informative. Given the numerous uncertainties
364 (from the observation side: spectral slopes calculated from spectra very close, but still not
365 perfectly equal, to the true surface albedos; from the modeling side: arbitrary choice for grain
366 size and type of mixtures), it is not possible to discriminate between intimate or linear
367 mixtures of water ice and tholins, though both or a combination of the two are still compatible
368 with the observed spectral slopes. However, the general trend of the modeled spectral slopes
369 leaves less ambiguity and advocates for a strong gradient in water ice/solid organics content
370 between the two observed units. This unequivocally confirms the interpretation that "dark
371 brown" terrains are largely dominated by solid organics similar to atmospheric aerosols, and
372 also validates the enrichment in the fine-grained water ice content (or the pure water ice larger
373 exposure) of the "dark blue" regions relative to the "dark brown" terrains (as suspected from
374 the spectral slopes extracted from atmosphere-corrected Titan's spectra by Rodriguez et al.,
375 2006; from uncorrected spectra by Soderblom et al., 2007; Barnes et al., 2008; Clark et al.,
376 2010; in accordance with radiative transfer modeling of Hirtzig et al., 2013).

377

378 **3. Discussion.**

379 Putting together the distribution of Titan's dunes inferred from the RADAR images
380 and the mapping of the VIMS observations, it is possible to confirm and quantify, at the
381 global scale, the correlation between the dune regions and the infrared "dark brown" unit. We

discuss here the possible implications of such a correlation for the sand composition, the volume of the solid organic trapped in the dunes and the climatology.

3.1 Latitudinal distribution of RADAR-mapped dunes and correlation with VIMS spectral units.

Figure 4 shows the fractional surface area occupied by Titan's dunes observed by the RADAR as a function of latitude, updating and extending that of Le Gall et al. (2011). The dune surface area has been normalized by the total fractional area imaged by the RADAR (including SAR and HiSAR observations), in such a way that the calculation of fraction of dune coverage is not biased by the partial coverage of the RADAR observations. The latitudinal distribution of dunes is Gaussian-like to first order with a maximum fractional coverage of ~60% at the equator, dropping down to no dunes for latitudes higher than ±30°. The only exceptions are a few dunes found at ~40°S and ~50°N within isolated small areas morphologically (greater interdune areas) and spectrally (brighter at radar and infrared wavelengths) distinct from the majority of those observed around the equator (see Radebaugh et al., 2012).

This particular distribution of the dunes, generally associated with arid to semi-arid climates (e.g. Lancaster, 1995), strongly suggests that the efficiency of the sediment mobility monotonically decreases with latitude, possibly due to increasing ground humidity from the equator to the poles resulting in a declining availability in mobile sediment (Le Gall et al., 2012). Those observations are in general agreement with climate models that predict a global transport of humidity from the equator to the poles, inescapably drying the equatorial regions where arid conditions must prevail (Rannou et al., 2006; Mitchell et al., 2006, 2008;

405 Schneider et al., 2012). The progressive poleward disappearance of dunes could also be partly
406 attributed to a decrease in availability of "dark brown" organic sediment (mid-latitudes being
407 indeed dominated by bright infrared terrains, cf. **Figure 2a**) and to less frequent storms able to
408 produce sufficiently strong winds to mobilize the sediment (Schneider et al., 2012). Looking
409 more carefully, the latitudinal distribution of dunes displays a slight hemispherical imbalance
410 with fewer dunes in the southern hemisphere. If infrared bright equatorial terrains are more
411 elevated than the equatorial "basins" where dunes seem to preferentially accumulate (Le Gall
412 et al., 2012), this slight south/north asymmetry could be explained by the topography, because
413 most of these highlands (equatorial bright terrains) are located in the southern hemisphere
414 (Lorenz et al., 2013).

415 We also indicate in **Figure 4** the latitudinal fractional coverage of the VIMS "dark
416 brown" unit inferred from the global VIMS spectral unit map (**Figure 2b**). The latitudinal
417 correspondence between the fractional coverage of the VIMS "dark brown" unit and the
418 RADAR-mapped dunes is very good. The two distributions can be almost super-imposed,
419 pointing toward a very high level of correlation between the dunes and the VIMS "dark
420 brown" unit. The precise degree of spatial correlation is explored and quantified in the
421 following section.

422 The latitudinal extent of the "dark brown" unit leads to an important conclusion. The
423 infrared spectral signature of the bright mid-latitudes seems to indicate that sand has not
424 settled in large exposed amounts at mid-latitudes in the present epoch. If the sand came from
425 high latitudes, it must have been swept efficiently to the equatorial belt without leaving a lot
426 en route in mid-latitudes. Another possibility is that the sand was never deposited away from
427 the equator, which raises the questions of where it came from and how it formed.

428

[Figure 4 – single column]

3.2 Global geographic correlation between RADAR-mapped dunes and VIMS spectral units, dune global coverage and total sand volume: implication for Titan's global carbon cycle.

[Figure 5 – full page, landscape]

We show in **Figure 5** (bottom) the spatial overlap between the dune fields extracted from the RADAR observations (see **Figure 1b**) and the "dark brown" and "dark blue" units derived from the VIMS global map (see **Figure 2b**). We observe a noticeably good correlation between the imaged dunes and the VIMS "dark brown" unit, extending at the global scale their very good latitudinal correlation (**Section 3.1** and **Figure 4**). Local visual examination (**Figure 5**, top insets for examples) shows that the edges of dune fields match most of the boundaries of the "dark brown" unit to within the resolution limit of the data.

Quantitative correlation calculations show that 72 ± 3% of the imaged dunes (SAR and HiSAR with spatial sampling down to ~2 km/pixel) lie in the "dark brown" unit. Conservative uncertainties have been computed taking into account (1) the visual 2% error in drawing the boundaries of the RADAR dune fields (see **section 2.1**), (2) the 1.5% and 0.5% errors in estimating the areas covered by the "dark brown" and "dark blue" units respectively (caused by the low-resolution VIMS observations in some places and the resulting difficulty in visual identification of a sharp border for the more diffuse parts of the "dark brown" and "dark blue"

451 units – see **section 2.2**), and (3) co-registration errors due to remaining uncertainties on
452 Titan's orbital parameters and Cassini pointing, leading to a global shift between RADAR and
453 VIMS datasets which has been estimated to 0.5° at maximum (mostly in longitude).

454 The geographic overlap between RADAR-mapped dunes and the VIMS "dark brown"
455 unit is substantial and indicates that dune material composition is largely dominated by solid
456 organics (see **section 2.2**). Conversely, the correlation of dunes with the "dark blue" unit is
457 much more fortuitous (2 ± 1% of the observed dunes being infrared-"dark blue"). Only a few
458 "dark blue" patches among the whole "dark blue" unit are found within the dune fields. But,
459 even if incidental, the occurrence of such "dark blue" areas in dune regions may be very
460 informative regarding the local heterogeneities in composition, morphological and/or textural
461 properties of the dunes. We showed in **section 2.2** that the spectra modeling strongly favors
462 local enrichment in water-ice of a solid organic-water ice granular mixture or a larger
463 exposure percentage of pure water ice (i.e. a lack of sediments in the interdune areas) to
464 explain the spectral behavior of the "dark blue" dunes, as it was previously anticipated
465 (Barnes et al., 2008; Le Gall et al., 2011). This hypothesis is further supported by the fact that
466 the "dark blue" unit occurs quasi-systematically as diffuse patches at borders delimiting dark
467 and bright terrains, and may represents areas of intermediate organic sediment availability.
468 Finally, a few dune fields are also found outside of the "dark brown" and "dark blue" regions.
469 Most of them are isolated patches (also known as "cat scratches") surrounded by local reliefs
470 where dunes are shorter and present very bright interdune areas at the RADAR wavelength.
471 Those dune fields have probably interdune areas totally devoid of sediment, which make them
472 appearing also globally brighter in the infrared lower-resolution images rather than brown or
473 blue. **Figure 6** summarizes the actual interpretations of the dune infrared colors in terms of
474 dune field morphology and progressive decrease in sediment availability.

475

476 **[Figure 6 – single column]**

477

478 The high level of qualitative and quantitative spatial correlation between the dunes and
479 the "dark brown" unit that we infer from our global RADAR and VIMS maps confirms the
480 strong bilateral connection between these geomorphological and spectral units. We can thus
481 extrapolate with reasonably good confidence the extent of the dune fields (or at least the dune
482 material) to the total area of the VIMS "dark brown" spectral unit. Given the spectral
483 homogeneity of the "dark brown" unit, this also tells us that the dune material must be
484 homogeneous in composition and grain size (sand-sized solid organics) over the total extent
485 of the dune regions, in good agreement with the global homogeneity of the RADAR
486 reflectivity and emissivity of the dune fields (Janssen et al., 2011) and consistent with dune
487 formation processes. Therefore the dune system on Titan can be extended up to 17.5% of
488 Titan's surface area (see **Section 2.2**). This corresponds to an area of ~14.6 million km^2, much
489 less than the over-estimated ~18-19 million km^2 computed from the arbitrary extrapolation
490 using the RADAR observations alone (see **Section 2.1**).

491 We showed that the infrared "dark brown" unit is most likely dominated by solid
492 organics, equivalent to the material composing the RADAR-mapped dunes. However, as
493 infrared reflectivity of a surface is primarily sensitive to the composition and granularity of
494 the first tens of microns of the material coating it, the "dark brown" spectral class, where no
495 RADAR observations are available and where dunes cannot be resolved, may be caused by a
496 thin coating independent of the underlying geologic feature, i.e. with or without dunes. We
497 should therefore consider two possible alternative scenarios: either (1) the "dark brown" unit

498 is entirely covered by dunes, or (2), more conservatively, only the "dark brown" areas
499 overlapping RADAR-mapped dunes is covered by dunes, the rest of the "dark brown" unit
500 being coated by the dune material but without dune landforms (i.e. like sand sheets).

501 Considering an average dune height of 100 m (Barnes et al., 2008; Neish et al., 2010),
502 a dune/interdune coverage fraction of 35-60% (Savage et al., this issue), an average thickness
503 of sediment covering the interdune (or covering the "dark brown" areas devoid of dunes) of 5
504 m (Lorenz et al., 2008), supposing a prismatic shape for the dunes, and taking into account the
505 uncertainties on the surface areas of the RADAR-mapped dunes and "dark brown" unit, the
506 total volume of organic sediments should be within the range $3\text{-}4.4\times10^5$ km^3 for the scenario
507 (1) and $1.7\text{-}2.5\times10^5$ km^3 for the scenario (2).

508 Assuming a mass density of 800 kg.m^{-3} for the organic sand particles, this corresponds
509 to an equivalent of 136,000 to 350,000 GT (with an "average" value of 230,000 GT) of solid
510 organic trapped in the dune sediments. These estimates make the equatorial sand one of the
511 largest hydrocarbon reservoirs on Titan's surface and atmosphere, greater than the polar lakes
512 and seas (ranging from 4,000 to 30,000 GT, Lorenz et al., 2008; Sotin et al., 2012), the
513 photochemical haze particles (0.14 GT, Sotin et al., 2012), and possibly the current
514 atmospheric gases (190,000 GT, Sotin et al., 2012). Considerable subsurface reservoirs of
515 liquid or gaseous hydrocarbons may also exist on Titan (Hayes et al., 2008; Mousis and
516 Schmitt, 2008; Cornet et al., 2012; Choukroun and Sotin, 2012), but their volumes are still
517 impossible to evaluate.

518 Titan's atmospheric methane is irreversibly destroyed by solar photons and charged
519 particles accelerated by Saturn's magnetosphere. A large fraction of the atmospheric methane
520 destruction ends with the formation of complex organic aerosols that settle on the surface and
521 form the primary source of organic sediments from which dune formation may be initiated.

522 Taking our "average" value for the total mass of dune material and a formation rate for the
523 atmospheric aerosols of 10-130 kg/s (Rannou et al., 2003, 2004), the time required to form the
524 total amount of dune material from the settling of photochemical aerosols ranges from 50- to
525 730-Myr, consistent with the age of the last global outgassing episode proposed by the models
526 of Tobie et al. (2006), Mandt et al. (2012) and Choukroun and Sotin (2012), and the estimate
527 of the age of Titan's equatorial surface from crater counting (Wood et al., 2010; Neish and
528 Lorenz, 2012).

529

530 **4. Conclusions.**

531 This work has shown that a joint analysis of Cassini/RADAR and VIMS overlapping
532 observations is an extremely powerful tool to explore the surface of Titan, providing
533 additional constraints on the correlation between Titan's geomorphological and infrared
534 spectral units. By significantly updating mosaics of RADAR and VIMS observations of
535 Titan's surface, we were able to extract and delineate at the global scale both equatorial dunes
536 from RADAR images and infrared spectral units from VIMS hyperspectral images. A new
537 VIMS global mosaic corrected for the atmospheric contributions has been used in this study,
538 improving and extending the work of Soderblom et al. (2007), Barnes et al. (2008) and Le
539 Corre et al. (2008). RADAR-mapped dunes and the "dark brown" unit are similarly confined
540 within the equatorial belt (±30° in latitudes) with an equivalent distribution with latitudes.
541 This particular latitudinal distribution is indicative for the aridity of the climate prevailing at
542 Titan's tropics, characterized by lower ground humidity and more frequent (but still episodic)
543 energetic storms than at higher latitudes, increasing both sediment availability and mobility.
544 At the global scale, we found an overall correlation of 72% between the imaged dunes and the
545 equatorial infrared VIMS "dark brown" unit. The very high degree of global scale correlation

546 conclusively proves the close link between both units, which was already proposed based on
547 local studies (Soderblom et al., 2007; Barnes et al., 2008) and at the global scale from a
548 limited set of observations (Le Corre et al., 2008). This correlation allowed us to extrapolate
549 the extent of dune material to the whole surface area covered by the VIMS "dark brown" unit,
550 that is to say 14.6 ± 0.2 million km^2, updating and revising previous values evaluated using
551 the partial coverage of RADAR images alone. Spectral modeling confirms that Titan's dune
552 sediment (mostly "dark brown" in the infrared) is most plausibly largely dominated by solid
553 organics similar to the photochemical atmospheric aerosols.

554 A refined estimate of the global dune material volume and distribution is essential to
555 constrain Titan's total organic inventory and therefore to understand the carbon cycle on
556 Titan. From our estimate of the total surface area covered by dune material and assuming two
557 possible scenarios for the sand distribution (either the sand is (1) entirely trapped in dune
558 landforms, or (2) trapped in dunes at places where dune landforms are firmly observed and in
559 sand sheets elsewhere), we estimate the total volume of organic sand to be $1.7\text{-}4.4\times10^5$ km^3.
560 The average total amount of hydrocarbon trapped in Titan's sand is thus evaluated to 230,000
561 GT, confirming that dunes (and possibly sand sheets) are a major geological surface unit and
562 the largest visible hydrocarbon reservoir on Titan. The volume and the spectroscopic
563 properties of the sediment contained in Titan's dunes are consistent with organic products of
564 atmospheric origin. Given the rate of atmospheric methane destruction into organic aerosols,
565 we calculate a maximum age of 730 Myr for the dune material, which agrees with the
566 timeframe of the last episode of global methane outgassing (e.g. Tobie et al., 2006) and the
567 young age of Titan's surface from crater counting (e.g. Wood et al., 2010).

568 All the results and refinements of our study, regarding the nature, origin and global
569 distribution of Titan's dunes, not only can help the global circulation models to improve their

prescriptions for tropical surface albedos and stratospheric haze production rates, but also bring strong constraints on the latitudinal distribution of ground humidity and strength of the near-surface winds. All the mapping shapefiles produced for this study (RADAR SAR and HiSAR coverages, RADAR-mapped dunes and VIMS spectral units) are shared with the community and accessible through the following website: `http://aim172.aim.univ-paris-diderot.fr/WebGIS/TitanGIS.html`.

The Cassini spacecraft continues to observe Titan up to the planned end of the Solstice mission in May 2017 and record new RADAR and VIMS images. In particular, new RADAR and VIMS observations of the equatorial belt (up to the mid-latitudes) will complement the high-resolution and spectral coverage of this region. Yet, it is important to note that up to May 2017 the RADAR experiment will only acquire 8 new SAR swaths and most of them will pass above already observed equatorial regions, the major potential update above new equatorial (and "dark brown") regions being expected from the T113 pass in September 2015. The RADAR observations of Titan's dunes we compile in this paper are therefore almost complete for the Cassini's era.

Even so, more high-resolution VIMS observations at low- to mid-latitudes and better-quality corrections for atmospheric scattering and surface photometry are needed in order to sharpen the fuzziest edges of the "dark brown" unit and thus to improve their location. Future work will also consist in adding the ISS mosaics to the Titan's GIS. ISS provides images of Titan's surface at 0.93 µm with an overall better spatial resolution than VIMS (except when VIMS is observing at the closest approach), providing additional constraints on the global correlation of dunes with infrared-dark regions. Because water ice is bright at 0.93µm, ISS should be good at differentiating "dark brown" dunes from "dark blue" and "bright" deposits. All of this will better constrain both the nature and geographic distribution of Titan's sand and

its total volume, which are crucial for a more complete understanding of Titan's climatology of and hydrocarbon cycle. Finally, the nature and origin of the singular infrared-"bluish" and "bright" areas within the dune fields will also deserve further investigations.

Acknowledgements

We sincerely thank the RADAR and VIMS Operations and Science Teams for their dedication in implementing and reducing the observations. We thank A.G. Hayes for very helpful discussions. We thank the two anonymous reviewers for useful and constructive comments. We also acknowledge support by the CNES (France), the Institut National des Sciences de l'Univers (INSU Progamme National de Planétologie, France), the Agence Nationale de la Recherche (ANR projects "EXODUNES" n°12BS05001 and "APOSTIC" n°11BS56002, France), and the LabEx UnivEarths (PRES Sorbonne Paris Cité). Part of this work has been performed at the Jet Propulsion Laboratory, California Institute of Technology under contract with NASA.

References

Allison, M., 1992. A preliminary assessment of the Titan planetary boundary layer, pp.113-118 in B. Kaldeich (ed), Proceedings of the Symposium on Titan, Toulouse, France, 9 –12 September 1991, ESA SP-338, European Space Agency, Noordwijk, The Netherlands, 1992.

614 Anderson, J.A., Sides, S.C., Soltesz, D.L., Sucharski, T.L., Becker, K. J., 2004.
615 Modernization of the Integrated Software for Imagers and Spectrometers. Lunar Planet. Sci.
616 35, Abstract #2039 (The Leagues, TX, USA).

617

618 Arnold, K., Radebaugh, J., Le Gall, A., Turtle, E.P., Lorenz, R.D., Garcia, A., 2013. Total
619 sand volume estimates on Titan from Cassini SAR, HiSAR, and ISS. Lunar Planet. Sci. 44,
620 LPI Contribution No. 1719, p. 2457 (The Leagues, TX, USA).

621

622 Barnes, J.W., Brown, R.H., Soderblom, L., Buratti, B.J., Sotin, C., Rodriguez, S., Le Mouélic,
623 S., Baines, K.H., Clark, R., Nicholson, P., 2007. Global-scale surface spectral variations on
624 Titan seen from Cassini/VIMS. Icarus186, 242–258.

625

626 Barnes, J.W., Brown, R.H., Soderblom, L., Sotin, C., Le Mouélic, S., Rodriguez, S., Jaumann,
627 R., Beyer, R.A., Buratti, B.J., Pitman, K., Baines, K.H., Clark R.N., Nicholson, P.D., 2008.
628 Spectroscopy, morphometry, and photoclinometry of Titan's dunefields from Cassini/VIMS.
629 Icarus 195, Issue 1, 200-414. doi: 10.1016/j.icarus.2007.12.006

630

631 Barnes, J.W., Buratti, B.J., Turtle, E.P., Bow, J., Dalba, P.A., Perry, J., Brown, R.H.,
632 Rodriguez, S., Le Mouélic, S., Baines, K.H., Sotin, C., Lorenz, R.D., Malaska, M.J., McCord,
633 T.B., Clark, R.N., Jaumann, R., Hayne, P.O., Nicholson, P.D., Soderblom, J.M., Soderblom,
634 L.A., 2013. Precipitation-induced surface brightenings seen on Titan by Cassini VIMS and
635 ISS. Planetary Science, 2:1. doi:10.1186/2191-2521-2-1

636

637 Brown, M.E., Roberts, J.E., Schaller, E.L., 2010. Clouds on Titan during the Cassini prime
638 mission: A complete analysis of the VIMS data. Icarus 205, 571-580.

639

640 Brown, R.H., Baines, K.H., Bellucci, G., Bibring, J.-P., Buratti, B.J., Capaccioni, F., Cerroni,
641 P., Clark, R.N., Coradini, A., Cruikshank, D.P., Drossart, P., Formisano, V., Jaumann, R.,
642 Langevin, Y., Matson, D.L., McCord, T.B., Mennella, V., Miller, E., Nelson, R.M.,
643 Nicholson, P.D., Sicardy, B., Sotin, C., 2004. The Cassini Visual and Infrared Mapping
644 Spectrometer (VIMS) Investigation. Space Sci. Rev. 115, 111-168. doi: 10.1007/s11214-004-
645 1453-x

646

647 Buratti, B.J., Sotin, C., Brown, R.H., Hicks, M.D., Clark, R.N., Mosher, J.A., McCord, T.B.,
648 Jaumann, R., Baines, K.H., Nicholson, P.D., Momary, T., Simonelli, D.P., Sicardy, B., 2006.
649 Titan: Preliminary results on surface properties and photometry from VIMS observations of
650 the early flybys. Planet. Space Science 54, Issue 15, 1498-1509. doi:
651 10.1016/j.pss.2006.06.015

652

653 Choukroun, M., Sotin, C., 2012. Is Titan's shape caused by its meteorology and carbon cycle?
654 Geophys. Res. Lett. 39, L04201.

655

656 Clark, R.N., Curchin, J.M., Barnes, J.W., Jaumann, R., Soderblom, L.A., Cruikshank, D.P,
657 Brown, R.H., Rodriguez, S., Lunine, J., Stephan, K., Hoefen, T.M., Le Mouélic, S., Sotin, C.,

Baines, K.H., Buratti, B.J., Nicholson, P.D., 2010. Detection and Mapping of Hydrocarbon Deposits on Titan. J. Geophys. Res. 115, E10005. doi: 10.1029/2009JE003369

Cornet, T., Bourgeois, O., Le Mouélic, S., Rodriguez, S., Lopez Gonzalez, T., Sotin, C., Tobie, G., Fleurant, C., Barnes, J.W., Brown, R.H., Baines, K.H., Buratti, B.J., Clark, R.N., Nicholson, P.D., 2012. Geomorphological significance of Ontario Lacus on Titan: Integrated interpretation of Cassini VIMS, ISS and RADAR data and comparison with the Etosha Pan (Namibia). Icarus 218, Issue 2, 788 – 806. doi:10.1016/j.icarus.2012.01.013

Cornet, T., Le Mouélic, S., Rodriguez, S., Sotin, C., Bourgeois, O., Lefèvre, A., Barnes, J.W., Brown, R.H., Baines, K.H., Buratti, B.J., Clark, R.N., Nicholson, P.D., 2013. Estimates of Titan's Surface Photometry in the 5 Microns Atmospheric Window Using the Cassini Visual and Infrared Mapping Spectrometer (VIMS). Lunar Planet. Sci. 44, LPI Contribution No. 1719, p. 2048 (The Leagues, TX, USA).

Elachi, C., Allison, M.D., Borgarelli, L., Encrenaz, P., Im, E., Janssen, M.A., Johnson, W.T.K., Kirk, R.L., Lorenz, R.D., Lunine, J.I., Muhleman, D.O., Ostro, S.J., Picardi, G., Posa, F., Rapley, C.G., Roth, L.E., Seu, R., Soderblom, L.A., Vetrella, S., Wall, S.D., Wood, C.A., Zebker, H.A., 2004. Radar: The Cassini Titan Radar Mapper. Sci. Rev. 115, 71–110. doi: 10.1007/s11214-004-1438-9

679 Elachi, C., Wall, S., Janssen, M., Stofan, E., Lopes, R., Kirk, R., Lorenz, R.D., Lunine, J.I.,
680 Paganelli, F., Soderblom, L.A., Wood, C., Wye, L., Zebker, H., Anderson, Y., Ostro, S.,
681 Allison, M., Boehmer, R., Callahan, P., Encrenaz, P., Flamini, E., Francescetti, G., Gim, Y.,
682 Hamilton, G., Hensley, S., Johnson, W., Kelleher, K., Muhleman, D., Picardi, G., Posa, F.,
683 Roth, L., Seu, R., Shaffer, S., Stiles, B., Vetrella, S., West, R., 2006. Titan Radar Mapper
684 observations from Cassini's T3 fly-by. Nature 441, Issue 7094, 709-713. doi:
685 10.1038/nature04786

686

687 Greeley, R., Iversen, J.D., 1985. Wind as a Geological Process on Earth, Mars, Venus and
688 Titan. Cambridge Planetary Science Series no. 4. Cambridge, London, New York, New
689 Rochelle, Melbourne, Sydney: Cambridge University Press.

690

691 Hapke, B., 1993. Theory of Reflectance and Emittance Spectroscopy. 1st ed., Cambridge
692 University Press, Cambridge, UK.

693

694 Hayes, A.G., Aharonson, O., Callahan, P., Elachi, C., Gim, Y., Kirk, R., Lewis, K., Lopes, R.,
695 Lorenz, R.D., Lunine, J.I., Mitchell, K., Mitri, G., Stofan, E., Wall, S., 2008. Hydrocarbon
696 lakes on Titan: Distribution and interaction with an isotropic porous regolith. Geophys. Res.
697 Lett. 35, L09,204. doi:10.1029/2008GL033409

698

699 Hirtzig, M., Bézard, B., Lellouch, E., Coustenis, A., de Bergh, C., Drossart, P., Campargue,
700 A., Boudon, V., Tyuterev, V., Rannou, P., Cours, T., Kassi, S., Nikitin, A., Wang, L.,

Rodriguez, S., Le Mouélic, S.. Titan's surface and atmosphere from Cassini/VIMS data with updated methane opacity. Icarus 226, 470–486. doi: 10.1016/j.icarus.2013.05.033

Janssen, M.A., Le Gall, A., Wye, L.C., 2011. Anomalous radar backscatter from Titan's surface? Icarus 212, Issue 1, 321-328. doi: 10.1016/j.icarus.2010.11.026

Khare, B.N., Sagan, C., Arakawa, E.T., Suits, F., Callcott, T.A., Williams, M.W., 1984. Optical constants of organic tholins produced in a simulated titanian atmosphere: from soft X-ray to microwave frequencies. Icarus 60, 127-137.

Kok, J., Parteli, E.J.R., Michaels, T.I., Karam, D.B., 2012. The physics of wind-blown sand and dust. Reports on Progress in Physics 75, 106901. doi:10.1088/0034-4885/75/10/106901

Lancaster, N., 1995. Geomorphology of Desert Dunes. Routledge, London.

Lebonnois, S., Rannou, P., Hourdin, F., 2009. The coupling of winds, aerosols and chemistry in Titan's atmosphere. Phil. Trans. R. Soc. A 367, 665–682. doi:10.1098/rsta.2008.0243.

719 Le Corre, L., Le Mouélic, S., Sotin, C., Barnes, J.W., Brown, R.H., Baines, K.H., Buratti,
720 B.J., Clark, R.N., Nicholson, P.D., 2008. Global map of Titan's dune fields. European
721 Planetary Science Congress, Proceedings of the conference in Münster, Germany, p. 667.

722

723 Le Gall, A., Janssen, M.A., Wye, L.C., Hayes, A.G., Radebaugh, J., Savage, C., Zebker, H.,
724 Lorenz, R.D., Lunine, J.I., Kirk, R.L., Lopes, R.M.C., Wal, S., Callahan, P., Stofan, E.R.,
725 Farr, T., and the Cassini Radar Team, 2011. Cassini SAR, radiometry, scatterometry and
726 altimetry observations of Titan's dune fields. Icarus 213, Issue 2, 608-624. doi:
727 10.1016/j.icarus.2011.03.026.

728

729 Le Gall, A., Hayes, A.G., Ewing, R., Janssen, M.A., Radebaugh, J., Savage, C., Encrenaz, P.,
730 and the Cassini RADAR Team, 2012. Latitudinal and altitudinal controls of Titan's dune field
731 morphometry. Icarus 217, Issue 1, 231-242. doi: 10.1016/j.icarus.2011.10.024

732

733 Le Mouélic, S., Paillou, P., Janssen, M.A., Barnes, J.W., Rodriguez, S., Sotin, C., Brown,
734 R.H., Baines, K.H., Buratti, B.J., Clark, R.N., Crapeau , M., Encrenaz, P., Jaumann, R.,
735 Geudtner, D., Paganelli, F., Soderblom, L.A., Tobie, G., Wall, S., 2008. Mapping and
736 interpretation of Sinlap crater on Titan using Cassini VIMS and RADAR data. J. Geophys.
737 Res. 113, E04003. doi:10.1029/2007JE002965

738

739 Le Mouélic, S., Rannou, P., Rodriguez, S., Sotin, C., Griffith, C., Le Corre, L., Barnes, J. W.,
740 Brown, R. H., Baines, K. H., Buratti, B. J., Clark, R. N., Nicholson P. D., Tobie, G., 2011.

741 Evolution the North Polar cloud on Titan monitored by The VIMS Imaging Spectrometer
742 onboard Cassini. Planet. Space Science 60, 86-92. doi 10.1016/j.pss.2011.04.006

743

744 Le Mouélic, S., Cornet, T., Rodriguez, S., Sotin, C., Barnes, J.W., Baines, K.H., Brown, R.H.,
745 Lefèvre, A., Buratti, B.J, Clark, R.N., Nicholson, P.D., 2012. Uniform global mapping of
746 Titan's surface in several infrared atmospheric windows. Planet. Space Science 73, Issue 1,
747 178-190. doi: 10.1016/j.pss.2012.09.008

748

749 Lorenz, R.D., 2013. Physics of Saltation and Sand Transport on Titan: A Brief Review. Icarus, in
750 press. doi: 10.1016/j.icarus.2013.06.023

751

752 Lorenz, R.D., Lunine, J.I., Grier, J.A., Fisher, M.A., 1995. Prediction of Aeolian Features on
753 Planets: Application to Titan Paleoclimatology. J. Geophys. Res. 88, 26,377-26,386.

754

755 Lorenz, R.D., Wall, S., Radebaugh, J., Boubin, G., Reffet, E., Janssen, M., Stofan, E., Lopes,
756 R., Kirk, R., Elachi, C., Lunine, J., Mitchell, K., Paganelli, F., Soderblom, L., Wood, C., Wye,
757 L., Zebker, H., Anderson, Y., Ostro, S., Allison, M., Boehmer, R., Callahan, P., Encrenaz, P.,
758 Ori, G.G., Francescetti, G., Gim, Y., Hamilton, G., Hensley, S., Johnson, W., Kelleher, K.,
759 Muhleman, D., Picardi, G., Posa, F., Roth, L., Seu, R., Shaffer, S., Stiles, B., Vetrella, S.,
760 Flamini, E., West, R., 2006. The sand seas of Titan: Cassini RADAR observations of
761 longitudinal dunes. Science 312, 724–727. doi: 10.1126/science.1123257

762

763 Lorenz, R.D., Mitchell, K.L., Kirk, R.L., Hayes, A.G., Aharonson, O., Zebker, H.A., Paillou,
764 P., Radebaugh, J., Lunine, J.I., Janssen, M.A., Wall, S.D., Lopes, R.M.C., Stiles, B., Ostro, S.,
765 Mitri, G., Stofan, E.R., 2008. Titan's inventory of organic surface materials. Geophys. Res.
766 Lett. 35, CiteID L02206. doi: 10.1029/2007GL032118

767

768 Mousis, O., Schmitt, B., 2008. Sequestration of ethane in the cryovolcanic subsurface of
769 Titan. Astrophys. J. 677, L67–L70.

770

771 Lorenz, R.D., Radebaugh, J., 2009. Global pattern of Titan's dunes: Radar survey from the
772 Cassini prime mission. Geophys. Res. Lett. 36, Issue 3, CiteID L03202. doi:
773 10.1029/2008GL036850

774

775 Lorenz, R.D., Stiles, B.W., Aharonson, O., Lucas, A., Hayes, A.G., Kirk, R.L., Zebker, H.A.,
776 Turtle, E.P., Neish, C.D., Stofan, E.R., Barnes, J.W., the Cassini RADAR Team, 2013. A
777 global topographic map of Titan. Icarus 225, 367–377. doi: 10.1016/j.icarus.2013.04.002

778

779 Lucey, P.G., 1998. Model near-infrared optical constants of olivine and pyroxene as a
780 function of iron content. J. Geophys. Res. 103, Issue E1, 1703-1713.

781

782 Mandt, K.E., Waite, J.H., Teolis, B., Magee, B.A., Bell, J., Westlake, J.H., Nixon, C.A.,
783 Mousis, O., Lunine, J.I., 2012. The 12C/13C ratio on Titan from Cassini INMS measurements

784 and implications for the evolution of methane. Astrophys. J. 749, Issue 2, 14. doi:
785 10.1088/0004-637X/749/2/160

786

787 Mitchell, J.L., Pierrehumbert, R.T., Frierson, D.M.W., Caballero, R., 2006. The dynamics
788 behind Titan's methane clouds. P. Natl Acad. Sci. USA 103, 18421-18426.

789

790 Mitchell, J.L., 2008. The drying of Titan's dunes: Titan's methane hydrology and its impact on
791 atmospheric circulation. J. Geophys. Res. 113, Issue E8, CiteID E08015.

792

793 Neish, C.D., Lorenz, R.D., Kirk, R.L., Wye, L.C., 2010. Radarclinometry of the sand seas of
794 Africa's Namibia and Saturn's moon Titan. Icarus 208, Issue 1, 385-394. doi:
795 10.1016/j.icarus.2010.01.023

796

797 Neish, C.D., Lorenz, R.D., 2012. Titan's global crater population: A new assessment. Planet.
798 Space Sci. 60, 26–33. doi: 10.1016/j.pss.2011.02.016

799

800 Radebaugh, J., Lorenz, R.D., Lunine, J.I., Wall, S.D., Boubin, G., Reffet, E., Kirk, R.L.,
801 Lopes, R.M., Stofan, E.R., Soderblom, L., Allison, M., Janssen, M., Paillou, P., Callahan, P.,
802 Spencer, C., and the Cassini RADAR Team, 2008. Dunes on Titan observed by Cassini
803 RADAR. Icarus 194, Issue 2, 690-703. doi: 10.1016/j.icarus.2007.10.015

804

805 Radebaugh, J., Lorenz, R.D., Wall, S.D., Kirk, R.L., Wood, C.A., Lunine, J.I., Stofan, E.R.,
806 Lopes, R.M.C., Valora, P., Farr, T.G., Hayes, A.G., Stiles, B., Mitri, G., Zebker, H., Janssen,
807 M., Wye, L., Le Gall, A., Mitchell, K.L., Paganelli, F., West, R.D., Schaller, E.L., and the
808 Cassini RADAR Team, 2011. Regional geomorphology and history of Titan's Xanadu
809 province. Icarus 211, Issue 1, 672-685. doi: 10.1016/j.icarus.2010.07.022

810

811 Radebaugh, J., Le Gall, A., Barnes, J.W., Lorenz, R.D., Lunine, J.I., Kirk, R.L., and the
812 Cassini RADAR Team, 2012. Stabilized dunes on Titan indicate changes in climate and
813 surface processes. Lunar Planet. Sci. 43, LPI Contribution No. 1659, p. 2224 (The Leagues,
814 TX, USA).

815

816 Rannou, P., McKay, C.P., Cabane, R.D., 2003. A model of Titan's haze of fractal aerosols
817 constrained by multiple observations. Planet. Space Sci. 51, 963-976.

818

819 Rannou, P., Hourdin, F., McKay, C.P., Luz, D., 2004. A couple dynamics-microphysics
820 model of Titan's atmosphere. Icarus 170, 443-462.

821

822 Rannou, P., Montmessin, F., Hourdin, F., Lebonnois, S., 2006. The latitudinal distribution of
823 clouds on Titan. Science 311, 201–205.

824

825 Rodriguez, S., Le Mouélic, S., Sotin, C., Clénet, H., Clark, R.N., Buratti, B.J., Brown, R.H.,
826 McCord, T.B., Nicholson, P.D., Baines K.H. and the VIMS science team, 2006.
827 Cassini/VIMS observations of the Huygens landing site on Titan. Planet, Space Sci. 54, 1510-
828 1523.

829

830 Rodriguez, S. Le Mouélic, S., Rannou, P., Tobie, G., Baines, K.H., Barnes, J.W., Griffith,
831 C.A., Hirtzig, M., Pitman, K.M., Sotin, C., Brown, R.H., Buratti, B.J., Clark, R.N., Nicholson,
832 P.D., 2009. Global circulation as the main source of cloud activity on Titan. Nature 459, 678-
833 682, doi:10.1038/nature08014.

834

835 Rodriguez, S., Le Mouélic, S., Rannou, P., Sotin, C., Brown, R. H., Barnes, J. W., Griffith,
836 C., A., Burgalat, J., Baines, K., H., Buratti, B. J., Clark, R. N., Nicholson, P. D., 2011.
837 Titan's cloud seasonal activity from winter to spring with Cassini/VIMS. Icarus 216, 89-110,
838 doi:10.1016/j.icarus.2011.07.031

839

840 Savage, C.J., Radebaugh, J., Christiansen, E.H., Lorenz, R.D., 2013. Implications of dune
841 pattern analysis for Titan's surface history. Icarus, in press.

842

843 Schneider, T., Graves, S.D.B., Schaller, E.L., Brown, M.E., 2012. Polar methane
844 accumulation and rainstorms on Titan from simulations of the methane cycle. Nature 481, 58-
845 61. doi:10.1038/nature10666

846

847 Soderblom, L.A., Kirk, R., Lunine, J.I., Anderson, J.A., Baines, K.H., Barnes, J.W., Barrett,
848 J.M., Brown, R.H., Buratti, B.J., Clark, R.N., Cruikshank, D.P., Elachi, C., Janssen, M.A.,
849 Jaumann, R., Karkoschka, E., Le Mouélic, S., Lopes, R.M., Lorenz, R.D., McCord, T.B.,
850 Nicholson, P.D., Radebaugh, J., Rizk, B., Sotin, C., Stofan, E.R., Sucharski, T.L., Tomasko,
851 M.G., Wall, S.D., 2007. Correlations between Cassini VIMS spectra and RADAR SAR
852 images: Implications for Titan's surface composition and the character of the Huygens probe
853 landing site. Planet. Space Sci. 55, Issue 13, 2025–2036. doi: 10.1016/j.pss.2007.04.014

854

855 Sotin, C., Jaumann, R., Buratti, B.J., Brown, R.H., Clark, R.N., Soderblom, L.A., Baines,
856 K.H., Bellucci, G., Bibring, J.-P., Capaccioni, F., Cerroni, P., Coradini, A., Cruikshank, D.P.,
857 Drossart, P., Formisano, V., Langevin, Y., Matson, D.L., McCord, T.B., Nelson, R.M.,
858 Nicholson, P.D., Sicardy, B., Le Mouélic, S., Rodriguez, S., Stephan, K., Scholz, C.K., 2005.
859 Release of volatiles from a possible cryovolcano from near-infrared imaging of Titan. Nature
860 438, Issue 7043, 786-789. doi: 10.1038/nature03596

861

862 Sotin, C., Lawrence, K.J., Reinhardt, B., Barnes, J.W., Brown, R.H., Hayes, A.G., Le
863 Mouélic, S., Rodriguez, S., Soderblom, J.M., Soderblom, L.A., Baines, K.H., Buratti, B.J.,
864 Clark, R.N., Jaumann, R., Nicholson, P.D., Stephan, K., 2012. Observations of Titan's
865 Northern lakes at 5 μm: Implications for the organic cycle and geology. Icarus 221, Issue 2, p.
866 768-786. doi: 10.1016/j.icarus.2012.08.017

867

868 Stofan, E.R., Elachi, C., Lunine, J.I., Lorenz, R.D., Stiles, B., Mitchell, K.L., Ostro, S.,
869 Soderblom, L.A., Wood, C., Zebker, H., Wall, S., Janssen, M., Kirk, R., Lopes, R., Paganelli,

F., Radebaugh, J., Wye, L., Anderson, Y., Allison, M., Boehmer, R., Callahan, P., Encrenaz, P., Flamini, E., Francescetti, G., Gim, Y., Hamilton, G., Hensley, S., Johnson, W.T.K., Kelleher, K., Muhleman, D., Paillou, P., Picardi, G., Posa, F., Roth, L., Seu, R., Shaffer, S., Vetrella, S., West, R., 2007. The lakes of Titan. Nature 445, 61- 64. doi:10.1016/S0019-1035(03)00125-8

Tobie, G., Lunine, J., Sotin, C., 2006. Episodic outgassing as the source of atmospheric methane on Titan. Nature 440, 61–64. doi: 10.1038/nature04497

Turtle, E.P., Perry, J.E., McEwen, A.S., DelGenio, A.D., Barbara, J., West, R., Dawson, D.D., Porco, C., 2009. Cassini imaging of Titan's high-latitude lakes, clouds, and south-polar surface changes. Geophys. Res. Lett. 36, L02,204. doi:10.1029/2008GL036186

Turtle, E.P., DelGenio, A.D., Barbara, J.M., Perry, J.E., Schaller, E.L., McEwen, A.S., West, R.A., Ray, T.L., 2011a. Seasonal changes in Titan's meteorology. Geophys. Res. Lett. 38, L03203. doi:10.1029/2010GL046266

Turtle, E.P., Perry, J.E., Hayes, A.G., Lorenz, R.D., Barnes, J.W., McEwen, A.S., West, R.A., Del Genio, A.D., Barbara, J.M., Lunine, J.I., Schaller, E.L., Ray, T.L., Lopes, R.M.C., Stofan, E.R., 2011b. Rapid and extensive surface changes near Titan’s equator: Evidence of April showers. Science 331, 1414-1417. doi:10.1126/science.1201063

892 Warren, S.G., 1984. Optical constants of ice from the ultraviolet to the microwave. Applied
893 Optics 23, No. 8, 1206-1225.

894

895 Wood, C.A., Lorenz, R.D., Kirk, R., Lopes, R.M.C., Mitchell, K.L., Stofan, E.R., and the
896 Cassini RADAR Team, 2010. Impact craters on Titan. Icarus 206, 334–344. doi:
897 10.1016/j.icarus.2009.08.021

898

899 **Table 1.** SAR and HiSAR observations of Titan's dune fields from TA through T77.

Flyby	Date	SAR swath coverage[b]	Dune coverage within the SAR swath[c]	Median of the swath spatial sampling [azimuth-range] (km/pixel)	Dune latitude range	Dune longitude range	Imaged dune fields[d]
T3	Feb. 15, 2005	2.11%	16.6%	0.33-0.44	1.5°N-22.5°N	6.2°W-118.9°W	F
T8	Oct. 28, 2005	2.08%	51.2%	0.3-0.42	18.1°S-5.6°S	41.8°E-176.6°E	B, SL
T13	Apr. 30, 2006	1.72%	17.9%	0.33-0.45	16.7°S-4.2°S	142.7°W-170.1°W	SL
T13 (H)[a]	Apr. 30, 2006	0.17%	39.1%	2.71-1.57	10.5°S-2.5°S	164.9°W-169.7°W	SL
T16	Jul., 22, 2006	2.05%	7.5%	0.31-0.41	14.4°N-25.9°N	140.9°W-149.6°W & 11.1°E-19.9°E	- A
T17	Sep. 7, 2006	0.28%	83.7%	0.26-0.28	2.5°N-14.9°N	32.4°W-66.8°W	F
T19	Oct. 6, 2006	2.22%	7.5%	0.3-0.41	5.3°S-25.6°N	30.2°E-45.3°E	S
T19 (H)	Oct. 6, 2006	0.33%	6.5%	0.61-1.19	6.8°N-10.2°N	49.5°E-54.8°E	S, B
T21	Dec. 12, 2006	1.54%	18.6%	0.31-0.34	19.5°S-13.8°N	61.9°E-84.9°E	-
T23	Jan. 13, 2007	2.05%	7.9%	0.3-0.42	21.1°S-53.7°N	0°-21.8°E & 0°-47.8°W	S F, A
T25	Feb. 22, 2007	2.07%	17.2%	0.28-0.4	20.8°S-31.2°N	27.6°W-50.5°W	F, A
T28	Apr. 10, 2007	2.18%	38.3%	0.29-0.47	18.9°S-33.4°N	17.8°W-13.8°W	F, A
T29	Apr. 26, 2007	1.99%	15.4%	0.29-0.42	3.6°S-24.8°N	24.4°W-39.4°W	F, A
T36 (H)	Oct. 2, 2007	0.47%	47.6%	0.76-1.04	11.4°S-16.6°N	153.1°E-172°E	SL
T39 (H)	Nov. 19, 2007	0.31%	2.7%	0.92-1	1.8°S-1.3°N	158.9°E-161.5°E	SL
T41	Feb. 22, 2008	2.16%	23.4%	0.29-0.46	28.6°S-12.7°N	141.4°E -174.8°W	SL
T41 (H)	Feb. 22, 2008	0.39%	40.3%	0.61-1.28	3°S-8.6°N	45.7°W-65.8°W	A
T43	May 12, 2008	2.23%	9.1%	1.46-1.06	0.9°N-26.2°N	153.4°E-133.3°W	SL
T44	May 28, 2008	2.11%	17.8%	0.28-0.46	4.9°S-21.1°N	146.7°E-140.9°W	SL
T48	Dec. 5, 2008	1.51%	22.1%	0.33-0.28	15.8°S-27.4°N	154.2°E-148.3°W	SL
T49	Dec. 21, 2008	1.24%	45.7%	0.3-0.44	22.6°S-23.3°N	81.5°E-105.5°E	B
T49 (H)	Dec. 21, 2008	0.25%	49.1%	1.88-0.86	7.5°S-10.7°N	75.7°E-87.7°E	S, B
T50	Feb. 7, 2009	0.81%	18.1%	0.28-0.27	37.2°S-14.5°N	33.3°E-59.2°E	S
T50 (G)	Feb. 7, 2009	0.61%	46.7%	2-2.42	8.9°S-0.2°S	81.8°E-109.1°E	B
T55	May 15, 2009	2.08%	18.5%	0.3-0.39	31.5°S-22.8°N	133.8°W-172.7°W	SL
T56	Jun. 6, 2009	2.05%	24.4%	0.3-0.39	30.2°S-22.5°N	128.8°W-165.3°W	SL
T57	Jun. 22, 2009	0.83%	8.2%	0.3-0.27	29.8°S-10.7°N	132.4°W-157.8°W	SL
T58	Jul. 8, 2009	1.96%	12.4%	0.29-0.38	16.1°S-5.6°N	136.8°W-151.2°W	SL
T61	Aug. 25, 2009	2.02%	40.3%	0.29-0.39	14.8°S-8.3°N	50.5°E-177.1°W	S-B-SL
T64	Dec. 28, 2009	1.08%	5.9%	0.31-0.35	12.1°N-16.5°N	146.6°E-149.7°E	-
T77	June 20, 2011	1.06%	72.0%	0.33-0.43	2.4°N-18.7°N	33.2°W-95.1°W	F
T84	Jan. 2, 2013	0.71%	15.5%	0.3-0.39	6.5°N-16.3°N	132.7E-148.4E	B
T91	May 23,2013	1.02%	1.9%	N/A	15.5°N-19.5°N	108.4E-112.9E	B
T92	July 10, 2013	2.03%	13.9%	N/A	31.8°S-19.4°N	112.1E-117.9E	B

900 [a] (H) and (G) indicate HiSAR swaths. [b] In percentage of Titan's total surface area, not
901 accounting for possible overlap between swaths. [c] In percentage of swath's total surface area,
902 not accounting for possible overlap between swaths. [d] If available, the names of the dune
903 field(s) imaged during each flyby are noted: A = Aztlan, B = Belet, F = Fensal, S = Senkyo,
904 SL = Shangri-La.

905

Figure 1. (a) Global mosaic of all the Cassini SAR and HiSAR swaths recorded from the beginning of the mission (July 2004) through the 92nd close flyby of Titan (July 2013). The swaths are reprojected using the simple cylindrical coordinate system. **(b)** Dune fields and "inselbergs" embedded within the dune fields are here outlined in yellow. The inset shows a zoomed view the RADAR map (**Figure 1a**) with an example of how dune fields are delineated, excluding the "inselbergs" and embedded bright areas.

Figure 2. (a) RGB color composite map of Titan's surface incorporating all VIMS observations between TA (October 26th, 2004) and T70 (June 21st, 2010). The RGB channels correspond to Red = 5.0 μm, Green = 2.01 μm and Blue = 1.27 μm, with the 5.0 μm image being corrected for photometry, and the 2.01 and 1.27 μm images being empirically corrected for scattering and photometry. The VIMS images are reprojected using the simple cylindrical coordinate system. **(b)** "Dark brown" and "dark blue" units are here represented by the solid brown and blue areas (details on how those spectral units have been extracted from the VIMS global map are explicated in the text).

Figure 3. (a) VIMS I/F spectra averaged over the whole "dark blue" (blue triangles) and "dark brown" (brown circles) units displayed in **Figure 2b**. The "dark blue" and "dark brown" spectra are averages of 25,129 and 466,819 spectra respectively. The I/F values are taken at the center of 5 atmospheric windows (at 1.27, 1.59, 2.01, 2.75 and 5 μm), each corrected for atmospheric haze scattering and surface photometry. **(b)** Scatter plot of the 1.27/1.59 vs 1.27/2.01 μm spectral slopes for all the "dark brown" (brown circles) and "dark blue" (blue triangles) spectra, all being empirically corrected for atmospheric scattering and

surface photometry. Squares denote the spectral slopes modeled for intimate (gray squares) or linear mixtures (black squares) of granular water ice and tholins by step of 10% of mixing, for grainsizes of 50 microns. The brown square is 100% of tholins and the blue square is 100% of water ice.

Figure 4. Dune and "dark brown" unit latitudinal distributions. The surface area covered by dunes is normalized by the surface area sampled by Cassini SAR and HiSAR (down to the spatial sampling of ~2 km/pixel) through T92, as a function of Titan's latitude (thick black curve). The latitude bin size is 1°. The dotted black line shows the fractional surface area of Titan covered by SAR+HiSAR swaths. It shows that all latitudes are significantly sampled by existing coverage.

Figure 5. (a) Maps of the dune fields (outlined by the yellow lines), "dark brown" regions (solid brown area) and "dark blue" regions (solid blue area), as extracted from the maps shown in **Figure 1b** and **2b**. **(b)** Zoom on the eastern part of the Shangri-La dune fields. **(c)** Zoom on the northern part of the Senkyo dune fields. **(d)** Zoom on the western part of the Shangri-La dune fields. The three insets illustrate the very good qualitative spatial correlation between the imaged dunes and the VIMS "dark brown" unit.

Figure 6. Sketch of Titan's dune sediment coverage related to their infrared color. "Dark brown" dune systems (dunes and interdunes) are dominated by organic sediment. "Dark blue" and "bright" dunes are gradually depleted and devoid of sediment in the interdune areas.

952 **Figures 1a and 1b.**

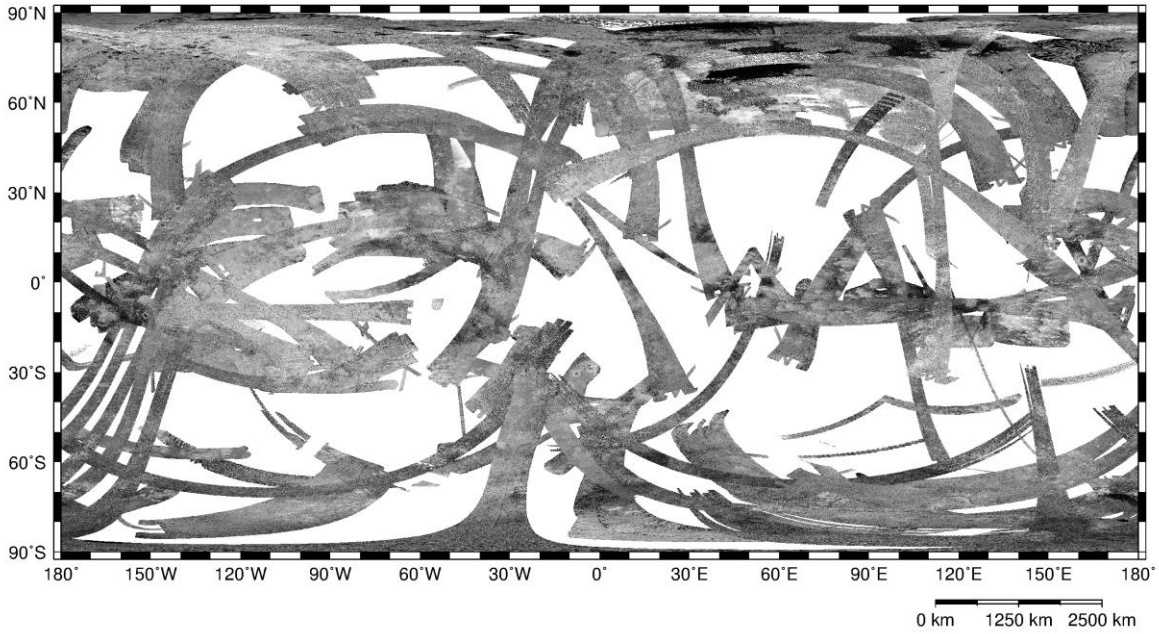

953

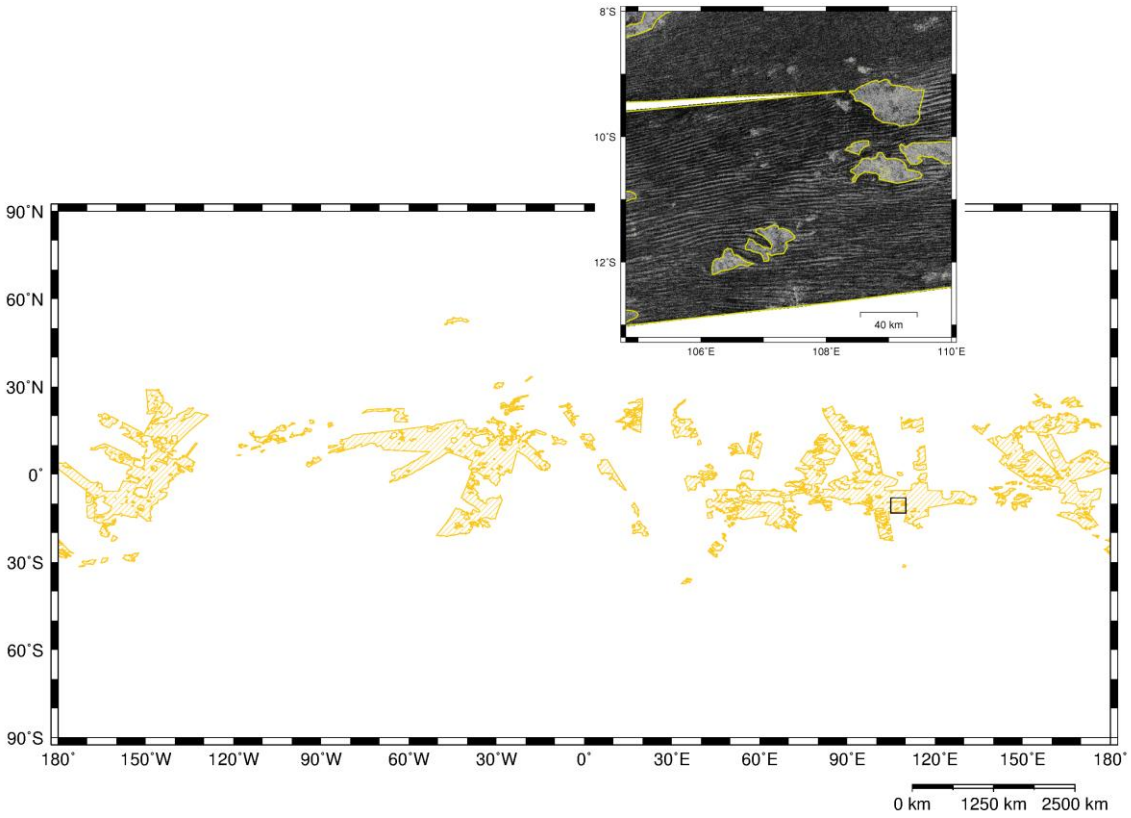

954

955

Figures 2a and 2b.

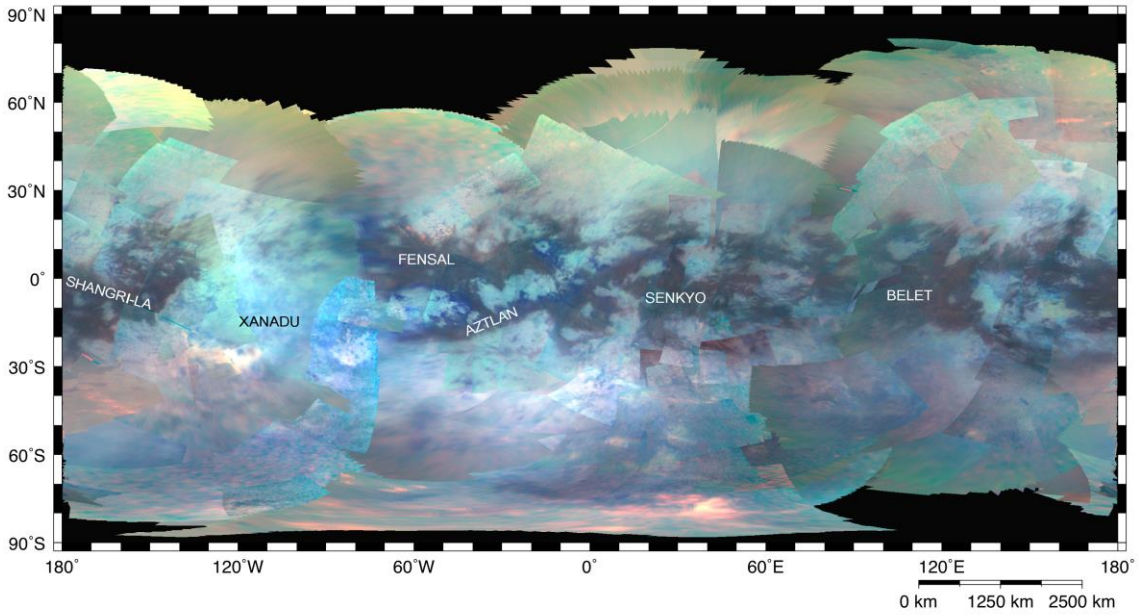

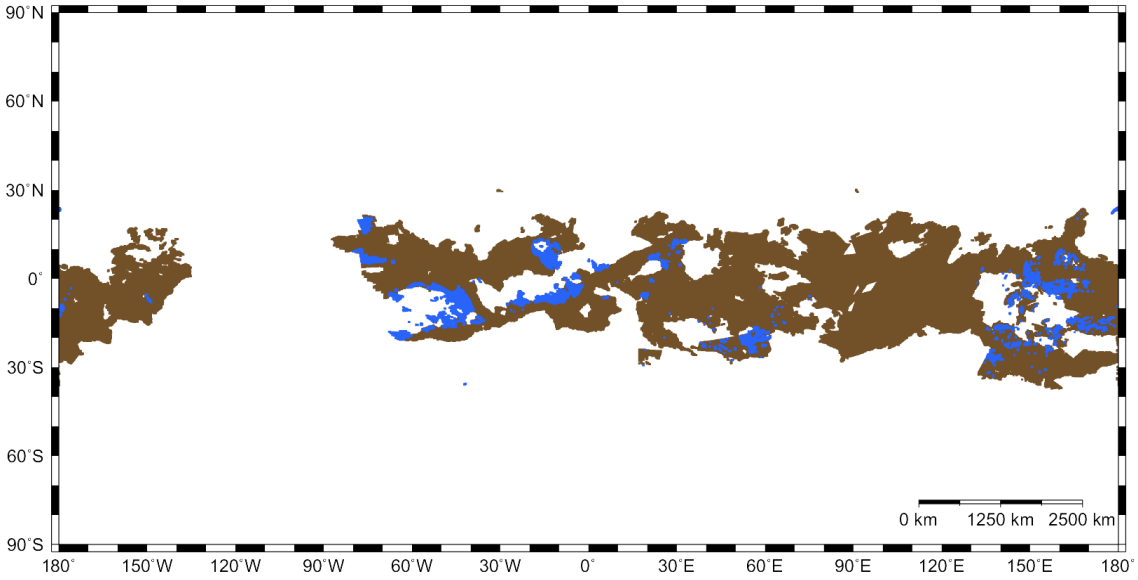

960 **Figures 3a and 3b.**

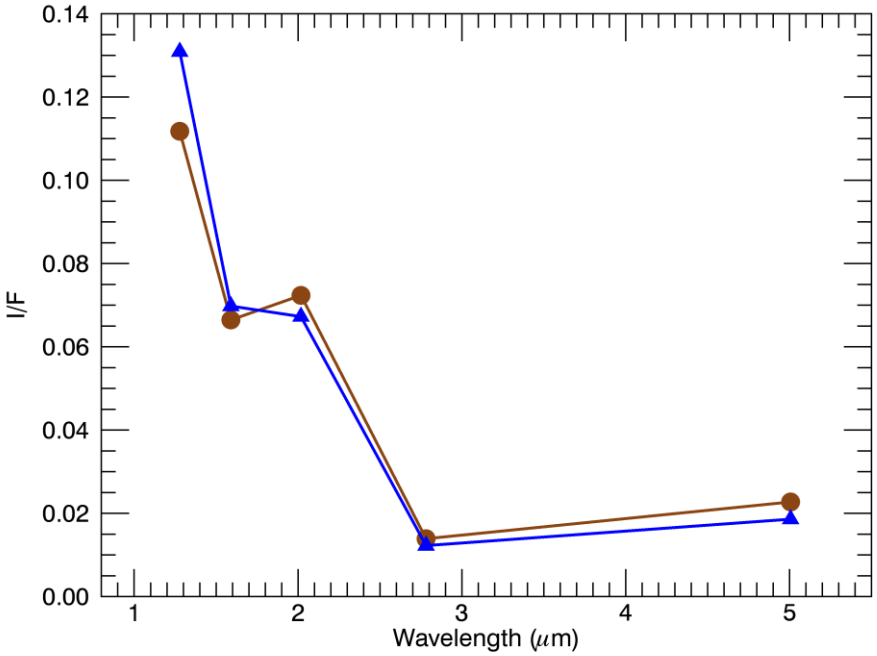

961

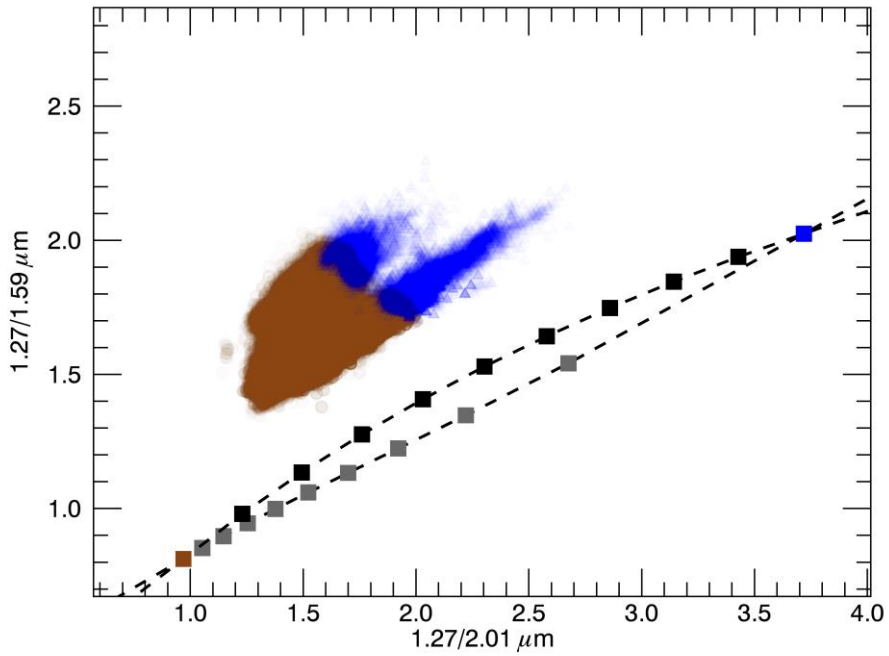

962

963 **Figure 4.**

964

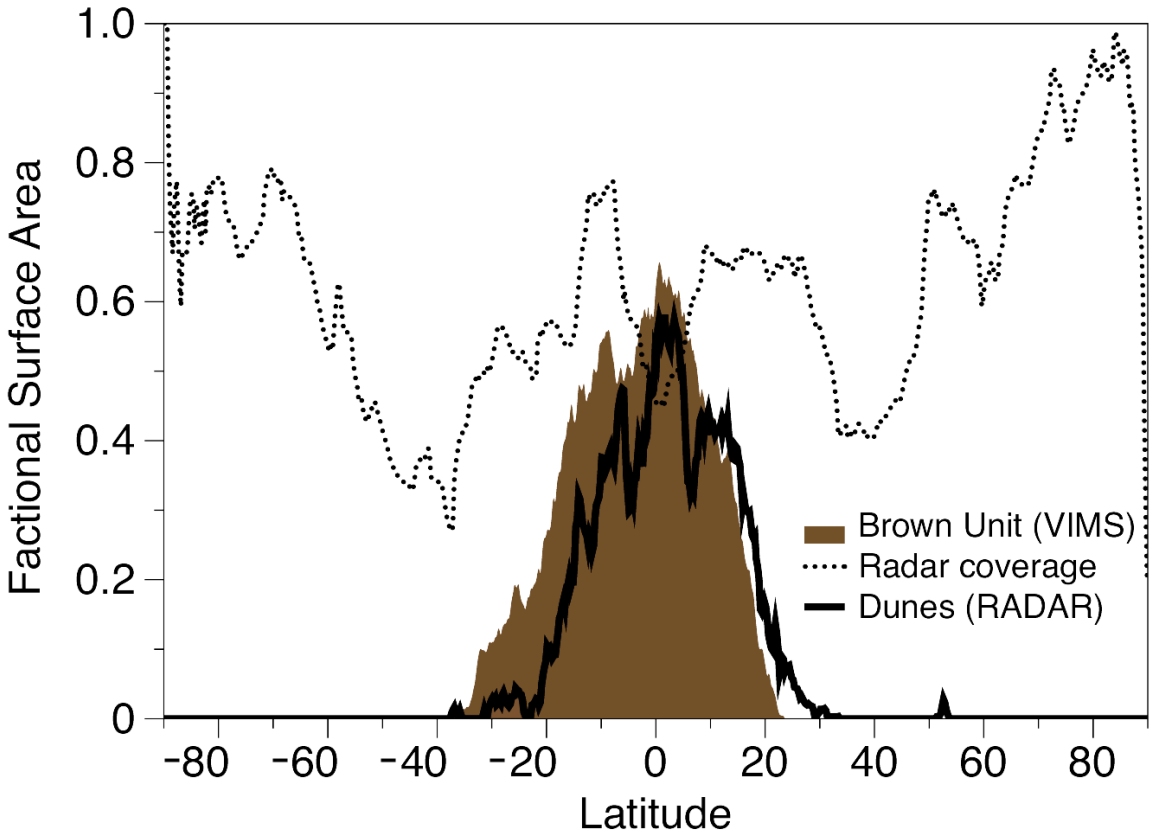

965

966

967 **Figure 5.**

968

969

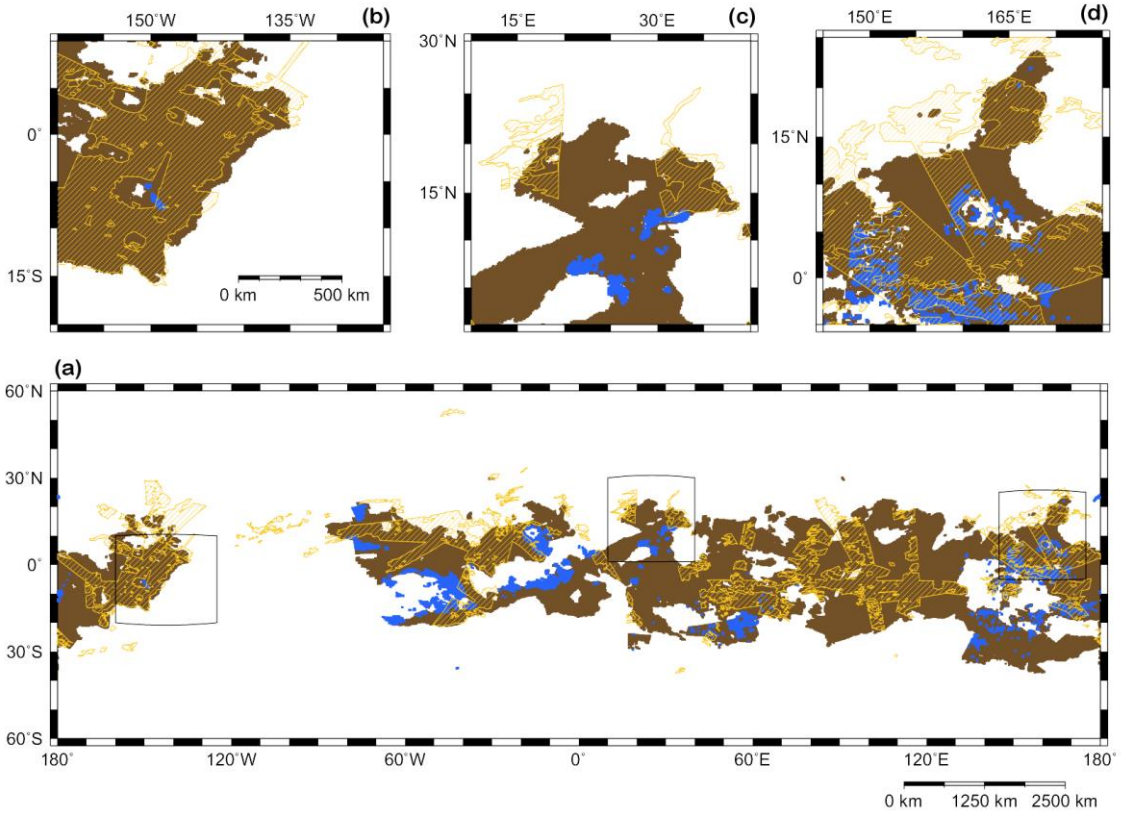

970

971

Figure 6.

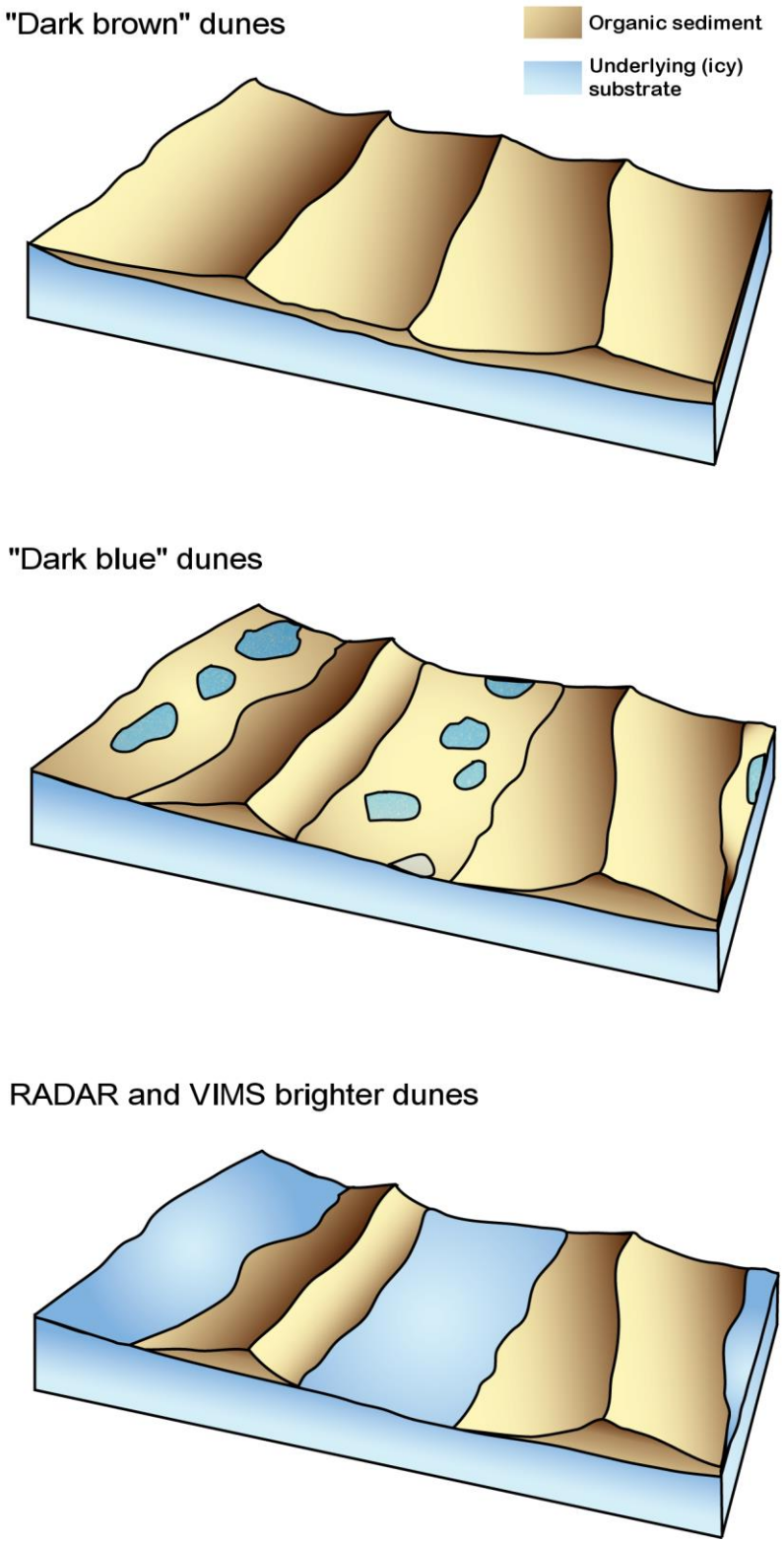
"Dark brown" dunes
Organic sediment
Underlying (icy) substrate
"Dark blue" dunes
RADAR and VIMS brighter dunes